ISSN: 2321-9653

INTERNATIONAL JOURNAL FOR RESEARCH IN APPLIED SCIENCE AND ENGINEERING TECHNOLOGY (IJRASET)

Fabrication of WS_2 Nanostructures Using Vapor Phase Deposition Method

[1]Vellachi. N

Assistant Professor, Physics Department, PSNA College of Engineering and Technology, Dindigul.

Abstract: ***Direct growth of atomically thin WS_2 nanoplates and nanofilms on the SiO_2/Si (300 nm) substrate by vapor phase deposition method without any catalyst is presented here. The WS_2nanostructures were systematically characterized by optical microscopy, scanning electron microscopy, Raman microscopy and atomic force microscopy. It is found that growth time and growth temperature play important roles in the morphology of WS_2 nanostructures. Moreover, by using Kelvin probe force microscopy, it is understood that the WS_2 nanoplates exhibit uniform surface and charge distributions less than 10 mV fluctuations. The results may apply to the study of other transition metal dichalcogenides by vapor phase deposition method.***

Key Words: ***Nanostructures, Thin film growth, Atomic force microscopy, Scanning electron Microscopy, Chemical exfoliation, Optoelectronics.***

1. INTRODUCTION

The emergence of graphene has drawn much attention due to its unique properties and potential applications [1-2]. Nevertheless, the absence of graphene band gap hinders its usefulness in field effect transistors because of the low current on/off ratio. Therefore, many other layered materials, such as boron nitride, and topological insulators, have been prepared and extensively studied [3]. Recently, layered transition metal dichalcogenides (MX_2 (M=Mo, W; X=S, Se) have attracted a great deal of attention for their wide applications in the field of optoelectronics [4-6], catalysis [7-10], energy [11-12] harvesting [8], and nano-electromechanical systems [13].

The WS_2 has a layered structure of S-W-S stacking layers made up from a basic unit cell, which is held together by van der Waals forces shown in fig 1(a). Recent investigations have demonstrated that WS_2-based devices have high performance with low power consumption at room temperature. The transition from indirect-to-direct band gap occurs when the dimension is reduced from bulk to monolayer, which shows promising applications in valleytronics and valley-based optoelectronics [14-15]. Therefore, the controllable nanostructure synthesis of these materials becomes essential. In this work, the studies are mainly focused on the synthesis and characterization of WS_2 nanostructures [16].

ISSN: 2321-9653

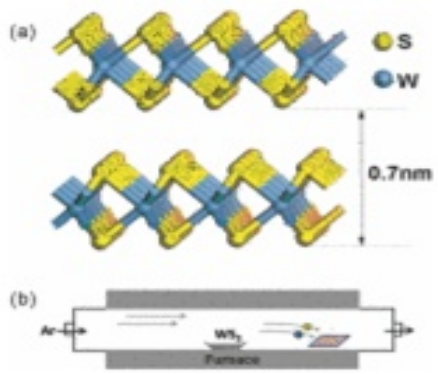

Figure 1. (a) Lattice structure of layered WS_2. (b) Schematic of CVD process for the growth of WS_2 nanostructures.

Currently, various methods have been employed to fabricate WS_2, including micromechanical cleavage technique [16], chemical exfoliation [17] and hydrothermal synthesis [18]. However, the thickness and size of the flakes are not controllable by these methods, which are infeasible for the integration of corresponding devices [19-21]. High quality WS 2 nanostructure synthesis remains challenging. Chemical vapor deposition (CVD) is the most expected method to synthesize single-layer, uniform and large scale WS 2 films. However, previous reports indicate that large areas of WS 2 thin films are mainly obtained by using WO 3, HS 2 or sulfur as the reactants [22-23].

A simple vapor phase deposition method for the growth of WS 2 nanostructures by decomposing WS 2 powder at high temperature is described here. WS 2 nanoplates as well as a large area of thin films were directly synthesized on SiO 2 substrate, and were systematically characterized. The electrostatic properties of WS 2 nanostructures were investigated by Kelvin probe force microscopy, which has been widely applied to other layered materials such as grapheme, MoS 2 and topological insulators [24]. The uniform surface and charge distributions provide insight into the electronic properties of these WS_2 nanostructure-based devices [25-27].

2. EXPERIMENTAL DETAILS

2.1. Synthesis of WS_2 nanostructures

WS_2 nanostructures were synthesized on the SiO_2/Si substrate in a horizontal tube furnace (Lindberg/Blue M) by vapor phase deposition method without any catalyst as shown in the reaction setup shown in fig 1(b). WS_2 powders (99.9%) were placed in the hot center of the furnace. The SiO_2/Si substrates cleaned with standard piranha solution were localized at the downstream zones 14 cm away (14-16 cm) from the hot center. The source material was heated to growth temperature (950–1000 °C) at a rate of 25 °C/min and maintained for an hour or half an hour before cooling down to room temperature naturally. During the procedure of the synthesis, the growth pressure was kept at 110 Pa within the 150 sccm Ar-H_2 gas flow (5% H_2).

2.2. Characterization

The morphologies of WS_2 nanostructures were characterized by scanning electron microscopy (SEM, JEOL,

JSM-6360) equipped with an energy dispersive X-ray spectrometer (EDX). Raman spectra were collected at room temperature in Renishaw micro-Raman spectrometer with 532 nm laser excitation light. The atomic force microscopy (AFM, SEIKO, SPI3800N + 300 HV) images were characterized to determine the thickness of WS_2 nanostructures. The electrostatic properties were investigated by Kelvin probe force microscopy (AFM, SEIKO, SPI3800N + 300 HV) under ambient conditions.

3. RESULT AND DISCUSSION

Fig 2(a) exhibits a SEM image of WS_2 samples, which were synthesized at 1000 °C and maintained for 30 mins. It can be clearly seen that triangular WS_2 nanoplates were fabricated on the SiO_2/Si substrate with lateral dimension up to several micrometers. And the elemental compositions of synthesized WS_2 nanoplates were determined by EDX analysis is given in fig 2(b). The atomic contents of S and W are 66.6%, 33.4%, respectively, which are in good agreement with the WS_2 formula and suggests successful fabrication of WS_2 nanoplates.

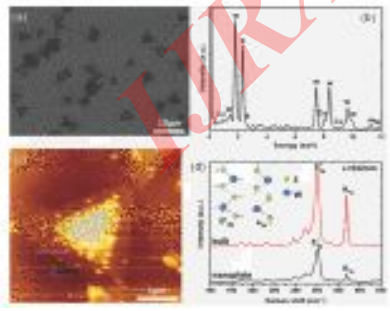

Figure 2(a) SEM image of triangular WS_2 nanoplates grown on SiO_2/Si subtrate. (b) EDX spectrum of synthesized WS_2 nanoplates. (c) AFM image of single WS_2 nanoplate. (d) Raman spectra of few-layer WS_2 nanoplates and bulk WS_2.

Fig 2(c) is the AFM image of a single triangular WS_2 nanoplate. The thickness is ~ 2.6 nm corresponding to 4 layers of WS_2, which indicates the successful synthesis of ultrathin nanoplates via vapor-solid mechanism. During the growth process, the WS_2powders were heated under high temperature and decomposed to W and S atoms, which recombined at the low temperature zone. At the initial growth stage, nucleation formed randomly on the SiO_2/Si substate. With the formation of the nucleation centers, the incoming W and S atoms tended to bond covalently with the edge of nucleation due to the dangling bonds existence. Therefore, the growth rate of lateral dimension is fast compared to the c-axis, resulting in the formation of nanoplate structure.

Raman spectroscopy was further performed to investigate the crystal structure and quality of few-layer WS_2 nanoplates. For the crystal structure of WS_2, there are 18 lattice dynamical modes: two dominant modes of E_{2g} and A_{1g} are investigated in the present work. The A_{1g} mode reflects the out-of-plane displacement of S atoms and the E_{2g} mode involves the in-plane displacement of W and S atoms. As shown in fig 2(d) , the E_{2g} and A_{1g} modes of few-layer WS_2 nanoplates have appeared at 349.7 cm^{-1} and 416.7 cm^{-1}, respectively. In contrast, the two modes of the WS_2 bulk are located at 350.3 cm^{-1} (E_{2g}) and 418.9 cm^{-1} (A_{1g}). A_{1g} mode

exhibits a blue-shift with the increase of the thickness due to the increasing van der Waals forces among layers, which is in good agreement with previous reports [23]. Raman results indicate high quality of synthesized WS_2 nanoplates.

To investigate the growth process of WS_2 nanostructures, the influences of growth time and temperature have been systematically conducted. When the growth time is prolonged to 60 mins under the experimental conditions mentioned above, it is seen that amounts of WS_2 nanoplates have been obtained and randomly distributed on the SiO_2/Si substrate. Fig 3(a) is the optical image: it clearly shows that some nanoplates merged together. The corresponding SEM image is shown in fig 3(b). Large areas of WS_2 nanofilms with several hundred micrometers were simultaneously fabricated as shown in the optical and SEM images fig 3 (c-d), which deposited on the same substrate with different distance compared with (a-b). By comparison, it can be concluded that the temperature is one of the factors, which influence the thickness and size of the WS_2 nanoplates. W nanowires with tens of micrometers were also obtained, which have been demonstrated by EDX analysis, further confirming the decomposition of WS_2 during the heating process.

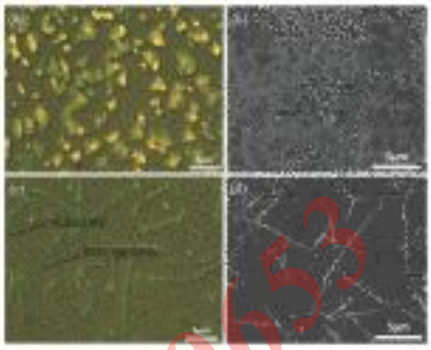

Figure 3(a) Photograph of few-layer WS_2 nanoplates on the SiO_2/Si substrate. (b) Corresponding SEM image. (c-d) Optical and SEM images of large area WS_2 films.

It is interesting that, when the growth temperature in the hot center was reduced to 950°C and the growth time has been maintained for 60 mins, the WS_2 nanoplates with random shape were synthesized (16–18 cm away from the hot center). Fig 4(a) shows the corresponding SEM image. Under such growth conditions, large areas of thin films were first grown on the whole substrate. Then the growth continues on the thin film, forming WS_2 nanostructures with random shapes. Fig 4(b) is a typical AFM image with the 0.5 nm surface roughness of the irregular WS_2 nanostructure. However, the surface roughness of the thin films is larger with 3 nm. Although the growth mechanism is not clear, the large areas of WS_2 nanostructure will benefit from the integration of WS_2-based devices.

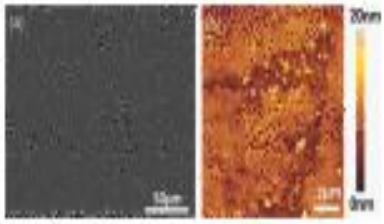

Figure 4(a) SEM image of irregular WS_2 nanofilms fabricated under 950 °C growth temperature. (b) Corresponding AFM image of WS_2 nanofilms.

WS_2 nanostructures present many promising applications in nanoelectronics and optoelectronics, [19-28], which have been extensively investigated. Nevertheless, there are few reported studies on the electrostatic properties of WS_2 and the interface between the WS_2 nanostructure and electrode, which are actually essential for the performance of WS_2-based devices. Herein, the electrostatic properties of the WS_2 nanostructures under ambient environment by employing Kelvin probe force microscopy were also studied. Fig 5(a) is the typical AFM image of the WS_2 nanostructures. Fig 5(b) is the corresponding surface potential image. The surface potential value of the WS_2 nanostructure is around 650 mV with 10 mV fluctuations across the whole area. The observation of the relatively homogeneous surface potential and charge distributions were observed, which also confirmed the high quality of the synthesized samples

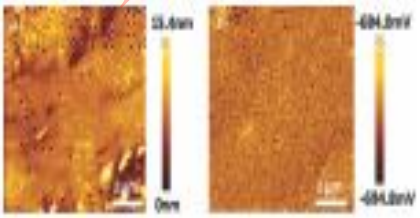

Figure 5 (a) A typical AFM image of WS_2 nanofilm. (b) Corresponding surface potential image.

Conclusion

Fabrication of the WS_2 nanostructures on the SiO 2/Si substrate via vapor phase deposition method without any catalyst is done this manner. The influence of growth time and temperature on the WS_2 nanostructures was investigated. The results demonstrate that the temperature is one of the important factors, which influence the thickness and size of the WS_2 nanoplates. While, the growth time mainly affect the quantity of the samples.

REFERENCES

1. A.K. Geim and K.S. Novoseloy, Nat. Mater. 6(3), pp. 183-191 (2007), http: //dx.doi.org/10.1038/nmat1849
2. J. Yu, L. Qin, Y. F. Hao, S. Y. Kuang, X. D. Bai, Y.-M. Chong, W. J. Zhang, and E. Wang, *ACS Nano* 4(1), 414–422 (2010).
3. X.-L. Qi and S.-C. Zhang, *Rev. Mod. Phys.* 83(4), 1057–1110 (2011).
4. G. L. Hao, X. Qi, Y. D. Liu, Z. Y. Huang, H. X. Li, K. Huang, J. Li, L. W. Yang, and J. X. Zhong, *J. Appl. Phys.* 111(11), 114312–114315 (2012).
5. M. Z. Hossain, S. L. Rumyantsev, K. M. F. Shahil, D. Teweldebrhan, M. Shur, and A. A. Balandin, *ACS Nano* 5(4), 2657–2663 (2011).
6. H. L. Zeng, J. F. Dai, W. Yao, D. Xiao, and X. D. Cui, *Nat. Nanotechnol.* 7(8), 490–493 (2012).
7. B. Radisavljevic, A. Radenovic, J. Brivio, V. Giacometti, and A. Kis, *Nat. Nanotechnol.* 6(3), 147–150 (2011).

8. S. F. Wu, J. S. Ross, G.-B. Liu, G. Aivazian, A. Jones, Z. Y. Fei, W. G. Zhu, D. Xiao, W. Yao, D. Cobden, and X. Xu, *Nat. Phys.*9(3), 149–153 (2013).
9. S. F. Wu, C. M. Huang, G. Aivazian, J. S. Ross, D. H. Cobden, and X. D. Xu, *ACS Nano* 7(3), 2768–2772 (2013).
10. T. F. Jaramillo, K. P. Jørgensen, J. Bonde, J. H. Nielsen, S. Horch, and I. Chorkendorff, *Science* 317(5834) 100–102, 2007.
11. C. Choi, J. Feng, Y. Li, J. Wu, A. Zak, R. Tenne, and H. Dai, *Nano Res.* 1–8 (2013).
12. A. Castellanos-Gomez, R. van Leeuwen, M. Buscema, H. S. J. van der Zant, G. A. Steele, and W. J. Venstra, *Adv. Mater.* 25, 899–903 , 2013.
13. W. Sik Hwang, M. Remskar, R. Yan, V. Protasenko, K. Tahy, S. Doo Chae, P. Zhao, A. Konar, H. Xing, A. Seabaugh, and D. Jena, *App. Phys. Lett.* 101(1), 013107 (2012).
14. W. J. Zhao, R. M. Ribeiro, M. Toh, A. Carvalho, C. Kloc, A. H. Castro Neto, and G. Eda, *Nano Lett.* 13(11), 5627–5634 (2013).
15. H. Zeng, G.-B. Liu, J. Dai, Y. Yan, B. Zhu, R. He, L. Xie, S. Xu, X. Chen, W. Yao, and X. Cui, *Sci. Rep.* 3 (2013).
16. H. S. S. Ramakrishna Matte, A. Gomathi, A. K. Manna, D. J. Late, R. Datta, S. K. Pati, and C. N. R. Rao, *Angew. Chem. Int. Ed.* 122(24), 4153–4156 (2010).
17. R. Huirache-Acuña, F. Paraguay-Delgado, M. A. Albiter, L. Alvarez-Contreras, E. M. Rivera-Muñoz, and G. Alonso-Núñez, *J. Mater. Sci.* 44(16), 4360–4369 (2009).
18. N. Perea-López, A. L. Elías, A. Berkdemir, A. Castro-Beltran, H. R. Gutiérrez, S. Feng, R. Lv, T. Hayashi, F. López-Urías, S. Ghosh, B. Muchharla, S. Talapatra, H. Terrones, and M. Terrones, *Adv. Funct. Mater.* 23(44), 5511–5517 (2013).
19. Y. Zhang, Y. F. Zhang, Q. Q. Ji, J. J. Ju, H. T. Yuan, J. P. Shi, T. Gao, D. L. Ma, M. X. Liu, Y. B. Chen, X. J. Song, H. Y. Hwang, Y. Cui, and Z. F. Liu, *ACS Nano* 7(10), 8963–8971 (2013).
20. Y.-H. Lee, L. L. Yu, H. Wang, W. J. Fang, X. Ling, Y. M. Shi, C.-T. Lin, J.-K. Huang, M.-T. Chang, and C.-S. Chang, *Nano Lett.*13(4), 1852–1857 (2013).
21. S. Tiefenbacher, H. Sehnert, C. Pettenkofer, and W. Jaegermann, *Surf. Sci.* 318(1–2), L1161–L1164 (1994).
22. A. Berkdemir, H. R. Gutierrez, A. R. Botello-Mendez, N. Perea-Lopez, A. L. Elias, C.-I. Chia, B. Wang, V. H. Crespi, F. Lopez-Urias, J.-C. Charlier, H. Terrones, and M. Terrones, *Sci. Rep.* 3(1755), 1–8 (2013).
23. Z. Q. Wei, D. B. Wang, S. Kim, S.-Y. Kim, Y. K. Hu, M. K. Yakes, A. R. Laracuente, Z. T. Dai, S. R. Marder, C. Berger, W. P. King, W. A. de Heer, P. E. Sheehan, and E. Riedo, *Science* 328(5984), 1373–1376 (2010).
24. G. L. Hao, Z. Y. Huang, Y. D. Liu, X. Qi, L. Ren, X. Y. Peng, L. W. Yang, X. L. Wei, and J. X. Zhong, *AIP Adv.* 3(4), 042125 (2013).
25. Y. Li, C.-Y. Xu, and L. Zhen, *Appl. Phys*
26. Y. Li, C.-Y. Xu, and L. Zhen, Appl. Phys. Lett. 102(14), 143110, 2013.
27. G. L. Hao, X. Qi, L. W. Yang, Y. D. Liu, J. Li, L. Ren, F. Sun, and J. X. Zhong, AIP Adv. 2(1), 012114 (2012).
28. T. Georgiou, R. Jalil, B. D. Belle, L. Britnell, R. V. Gorbachev, S. V. Morozov, Y.-J. Kim, A. Gholinia, S. J. Haigh, O. Makarovsky, L. Eaves, L. A. Ponomarenko, A. K. Geim, K. S. Novoselov, and A. Mishchenko, Nat. Nanotechnol. 8(2), 100–103 (2013).